

INHOMOGENEOUS MUSIG MODEL – A POPULATION BALANCE APPROACH FOR POLYDISPERSED BUBBLY FLOWS

E. Krepper¹, Thomas Frank², Dirk Lucas¹, H.-M. Prasser³, Ph. J. Zwart⁴

¹Forschungszentrum Dresden-Rossendorf, Institute of Safety Research
Germany-01328 Dresden, Bautzner Landstraße 128
E.Krepper@fzd.de; D.Lucas@fzd.de

²ANSYS Germany, ³ETH-Zürich, ⁴ANSYS Canada

ABSTRACT

A generalized inhomogeneous Multiple Size Group (MUSIG) Model based on the Eulerian modeling framework was developed in close cooperation of ANSYS-CFX and Forschungszentrum Dresden-Rossendorf and implemented into CFX-10. By simulating a poly-dispersed gas-liquid two-phase flow, the mass exchanged between bubble size classes by bubble coalescence and bubble fragmentation as well as the momentum exchange due to bubble size dependent bubble forces have to be considered. Particularly the lift force has been proven to play an important role for establishing a certain bubble size distribution dependent flow regime.

The derived model has been validated against experimental data from the TOPFLOW test facility at the Forschungszentrum Dresden-Rossendorf (FZD). The wire-mesh technology measuring local gas volume fractions, bubble size distributions and velocities of gas and liquid phases was applied. Numerous tests investigating air-water flow and steam-water flow at saturation conditions in vertical pipes having a length up to 8 m and a diameter up to 200 mm were performed and used for model validation. Furthermore in order to check the model framework for a more complex flow situation, further experiments on the flow field around a half moon shaped asymmetric obstacle were performed and the flow conditions were simulated by applying the inhomogeneous MUSIG model in direct comparison.

The paper describes the main concepts of the CFD model approach and presents model validation and application cases. The inhomogeneous MUSIG model approach was shown to be able to describe bubbly flows with higher gas content. Particularly the separation phenomenon of small and large bubbles, which was proven to be a key phenomenon for the establishment of the corresponding flow regime, is well described. Weaknesses in this approach can be attributed to the characterization of bubble coalescence and bubble fragmentation, which must be further investigated.

KEYWORDS

bubbly flow, CFD, non-drag forces, bubble breakup, bubble coalescence, population balance, validation

1. INTRODUCTION

Many flow regimes in Nuclear Reactor Safety Research are characterized by multiphase flows, with one phase being a continuous liquid and the other phase consisting of gas or vapour of the liquid phase. The flow regimes found in vertical pipes are dependent on the void fraction of the gaseous phase, which vary from bubbly flows at low fractions to higher void fraction regimes of slug flow, churn turbulent flow, annular flow and finally to droplet flow. In the regime of bubbly and slug flow the multiphase flow shows a spectrum of different bubble sizes. While disperse bubbly flows with low gas volume fraction are mostly mono-disperse, an increase of the gas volume fraction leads to a broader bubble size distribution due to breakup and coalescence of bubbles. Bubbles of different sizes are subject to lateral migration due to forces acting in lateral direction, which is different from the main drag force direction. Further the bubble lift force was found to change the sign as the bubble size varies. Consequently this lateral migration leads to a radial de-mixing of small and large bubbles and to further coalescence of large bubbles migrating towards the pipe center into even larger Taylor bubbles or slugs.

An adequate modeling approach has to consider all these phenomena. The paper presents a generalized inhomogeneous Multiple Size Group (MUSIG) Model based on the Eulerian modeling framework. Within this model the dispersed gaseous phase is divided into N inhomogeneous velocity groups (phases) and each of these groups is subdivided into M_j bubble size classes. Bubble breakup and coalescence processes between all bubble size classes M_j are taken into account by appropriate models.

2. NON DRAG FORCES AND INFLUENCE ON THE FLOW REGIME

Simulating a two-phase flow applying the Euler/Euler approach, the momentum exchange between the phases has to be considered. Apart from the drag acting in flow direction, the so called non-drag forces acting mostly perpendicular to the flow direction have to be considered. Namely the lift force, the turbulent dispersion force and the wall force play an important role. Here the influence of the lift force will be discussed.

2.1. Lift force inversion in a poly-disperse bubbly flow

The lift force considers the interaction of the bubble with the shear field of the liquid. Related on the unit volume it can be calculated as:

$$\vec{F}_L = -C_L \rho_l \alpha (\vec{w}_g - \vec{w}_l) \times \text{rot}(\vec{w}_l) \quad (1)$$

The classical lift force formulation for two-phase flows, which has a positive coefficient C_L , acts in the direction of decreasing liquid velocity. In case of co-current upwards pipe flow this is the direction towards the pipe wall. Numerical (Ervin and Tryggvason, 1997, Bothe et al., 2006) and experimental (Tomiyama et al., 1995) investigations showed, that the direction of the lift force changes its sign for gas-liquid flows, if a substantial deformation of bubbles occur. Tomiyama (1998) investigated single bubble motion and derived the following correlation for the coefficient of the lift force from these experiments:

$$C_L = \begin{cases} \min[0.288 \tanh(0.121 \text{Re}), f(Eo_d)] & Eo_d < 4 \\ f(Eo_d) & \text{for } 4 < Eo_d < 10 \\ -0.27 & Eo_d > 10 \end{cases} \quad (2)$$

with $f(Eo_d) = 0.00105Eo_d^3 - 0.0159Eo_d^2 - 0.0204Eo_d + 0.474$

This coefficient depends on the modified Eötvös number given by:

$$Eo_d = \frac{g(\rho_l - \rho_g)d_h^2}{\sigma} \quad (3)$$

Here d_h is the maximum horizontal dimension of the bubble. It is calculated using an empirical correlation for the aspect ratio by Wellek et al. (1966) with the following equation:

$$d_h = d_b \sqrt[3]{1 + 0.163Eo^{0.757}} \quad (4)$$

Figure 1 represents the dependency of C_L on the bubble size in eq. (2) for an air/water system at ambient conditions. For this case C_L changes its sign at a bubble diameter of $d_b = 5.8$ mm.

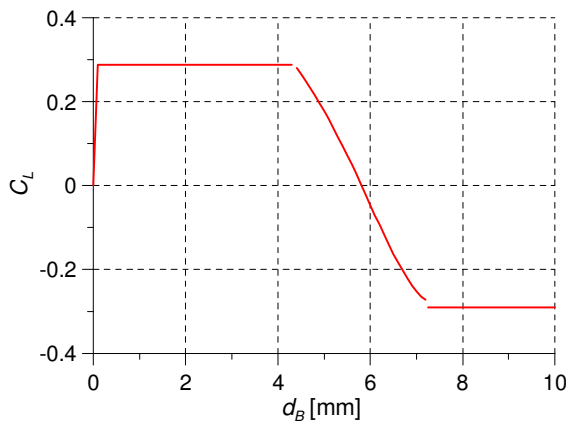


Figure 1: Lift coefficient for air-water bubbly flow according to eq. (2)

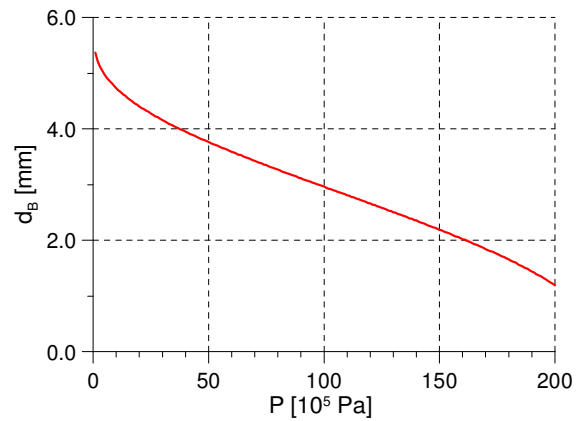


Figure 2: Decrease of the critical equivalent bubble diameter of the lift force sign change for steam-water bubbly flow vs. increasing saturation pressure

The MTLoop experiments performed at FZD (Prasser et al. 2002) have shown, that the lift force reverses in an evolving poly-disperse bubbly flow in an upward vertical pipe as well. Radial void fraction distributions show a wall peak for bubbles below the critical diameter, while bubbles with a larger diameter form a central void fraction peak. This is independent from the general type of the profile of the total void fraction, i.e. a wall-peak for the fraction of small bubbles is found also in case of a pronounced central peaked void fraction profile.

The FZD facility TOPFLOW has significantly extended the experimental opportunities to study this effect. It was shown that the described effects are present also in a large diameter pipe. The

vanishing of the wall peak in gas fraction profiles that are subdivided into narrow banded bubble-size classes of 0.5 mm class-width is observed at a diameter close to the value given by Tomiyama. For an air-water flow at ambient conditions, the equivalent critical bubble diameter is 5.5 mm. As shown in Fig. 3, bubbles of this size still display a pronounced wall peak, which is vanishing at about 6 - 6.5 mm bubble diameter. The fact that a volume fraction wall peak is still present for bubbles slightly larger than the Tomiyama diameter results from their continuous production close to the wall by coalescence events, which are quite frequent in the peak region and take place for bubbles below the critical size.

An important advantage of the TOPFLOW experiments is the possibility to check the correctness of the Tomiyama lift force model at high pressures and temperatures. The critical diameter is scaled by increases with the modified Eötvös number according eq. (3). Keeping in mind that the surface tension decreases with growing saturation temperature, the critical bubble diameter is expected to be lower for the steam-water tests. The dependency is given in Fig. 2. This was confirmed by the measurements, as shown in Fig. 3 (right side), where decomposed gas fraction profiles in the close-to-wall region are plotted for a saturation pressure of 6.5 MPa. A wall peak is only found for bubbles with diameters below 3.5 mm, which is in agreement with the dependency of the critical diameter from saturation pressure in Fig. 2.

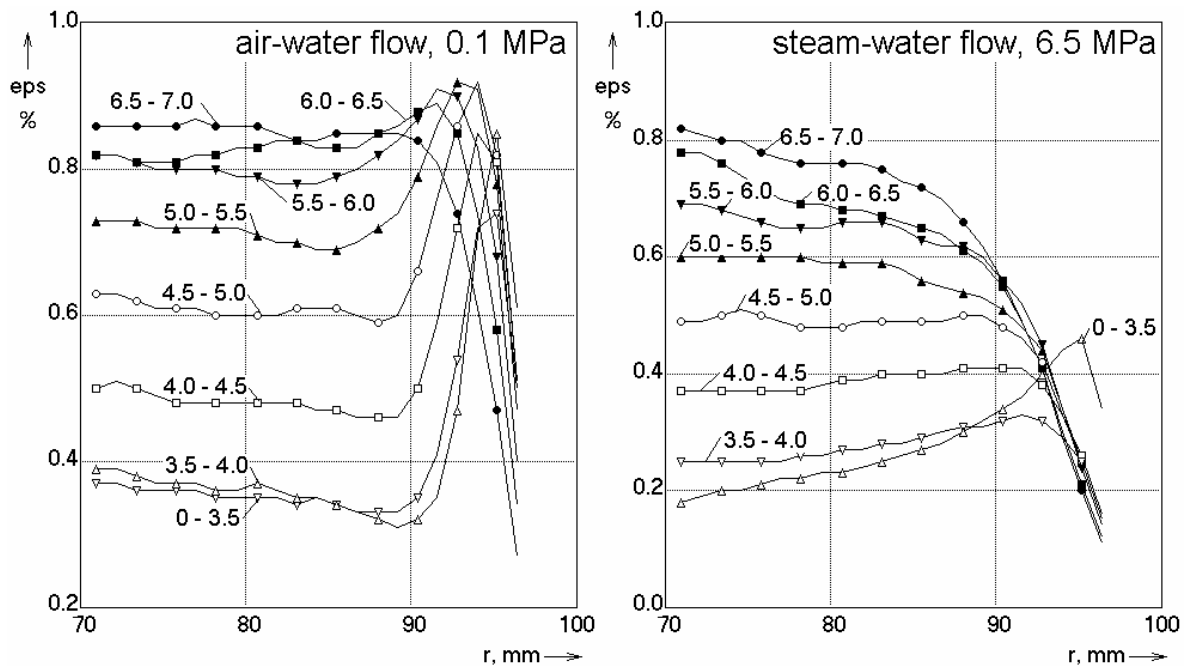


Figure 3: Gas fraction profiles decomposed according to bubble size classes in the test pipe DN200 at $J_L = 1.017$ m/s and $J_G = 0.219$ m/s, $L/D = 39.7$, gas injection orifices: $D_{inj} = 4$ mm (Prasser et al. 2007)

2.2. Development of the flow along a vertical pipe – radial separation of large and small bubbles

The evolution of the flow along the pipe is determined by a complex interaction between bubble forces, which cause a lateral bubble migration and bubble coalescence and breakup. Further the transition from bubbly to slug flow is influenced by this interaction. As mentioned above the lift force causes, that small bubbles (diameter < ca. 5.8 mm in case of air-water flow) can be found preferably in the wall region, while larger bubbles are accumulated in the core region. This separation of small and large bubbles clearly influences the development of the flow, since bubble coalescence and breakup depend on the local bubble densities (see Prince and Blanche 1990, Luo and Svendsen 1996). On the other hand the dissipation rate of turbulent energy is clearly larger in the near wall region than in the core flow. The consequences for the transition to slug flow can be explained by help of Fig. 4. An upward air-water flow is considered. In both considered cases small bubbles (diameter < 5.5 mm) are injected. In the left side of the figure a low superficial gas velocity was assumed. The small bubbles tend to move towards the wall. The local gas fraction in the wall region is larger than the averaged gas fraction, but it is still low. In this case bubble coalescence and breakup are in equilibrium and a stable bubbly flow is established.

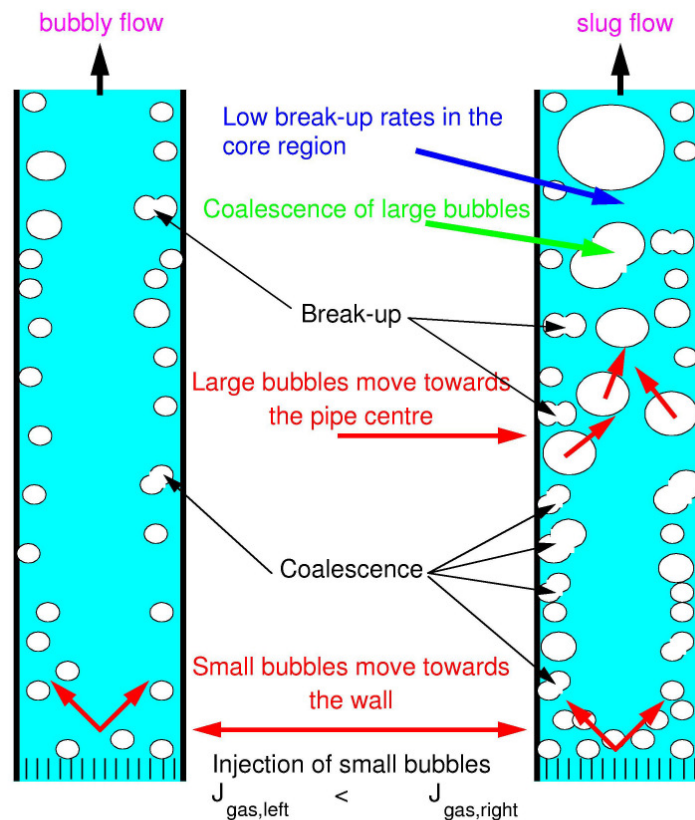


Figure 4: Stable bubbly flow (left) and transition to slug flow (right)

If the gas superficial velocity is increased (Fig. 4, right side), the equilibrium between bubble coalescence and breakup is shifted towards a larger bubble diameter, because the coalescence rate increases with the square of the bubble density, while the breakup rate is only proportional to the bubble density. The bubble breakup rate strongly increases with the bubble diameter.

By a further increase of the gas superficial velocity, more and more large bubbles (diameter > 5.5 mm) are generated. They start to migrate towards the pipe centre. If enough large bubbles are generated by coalescence in the wall region, some of them can reach the core region without further breakup. Because of the lower dissipation rate of turbulent energy they can then grow up by further coalescence at much lower breakup rates, typical for the low shear in the pipe centre.

This mechanism is the key for the transition from bubble to slug flow. That means, that for an appropriate modelling of the transition a number of bubble size classes as well as radial gas fraction profiles for each bubble size class and the lateral migration of differently sized bubbles have to be considered.

3. MULTIPLE SIZE GROUP APPROACH

3.1. The MUSIG model by Lo

For larger gas volume fractions, several bubble size classes have to be considered and the exchange of mass between them caused by bubble coalescence and breakup phenomena has to be taken into account. In principle, the Eulerian two-fluid approach as described above can be extended to simulate a continuous liquid phase and several gaseous dispersed phases solving the complete set of balance equations for each phase. The investigations however showed that for an adequate description of the gas volume fraction profile including a population balance model decades of bubble size classes would be necessary. In a CFD code, such a procedure is limited by the increased computational effort to obtain converged flow solutions.

To solve this problem, the multiple size group model first implemented by the code developers in CFX-4 solves only one common momentum equation for all bubble size classes (homogeneous MUSIG model, see Lo 1996). Mathematically, the Multiple Size Group model (MUSIG) is based on the population balance method and the two-fluid modeling approach. The dispersed phase is divided into M size fractions. The population balance equation is applied to describe the mass conservation of the size fractions taking into account of the inter-fraction mass transfer resulting from bubble coalescence and breakup. This model approach allows a sufficient number of size fraction groups required for the coalescence and breakup calculation to be used and has found a number of successful applications to large-scale industrial multiphase flow problems.

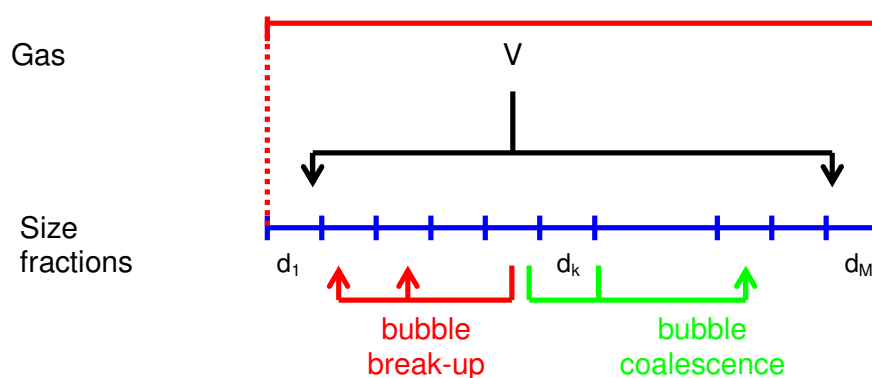


Figure 5: Schema of the standard MUSIG model: All size fractions representing different bubble sizes move with the same velocity field

Nevertheless, the assumption also restricts its applicability to homogeneous dispersed flows, where the slip velocities of particles are almost independent of particle size and the particle relaxation time is sufficiently small with respect to inertial time scales. Thus, the asymptotic slip velocity can be considered to be attained almost instantaneously. The homogeneous MUSIG model described above fails to predict the correct phase distribution when heterogeneous particle motion becomes important. One example is the bubbly flow in vertical pipes where the non-drag forces play an essential role on the bubble motion. In the previous chapter the lift force was described to change its sign, when applied for large deformed bubbles, which are dominated by the asymmetrical wake. The lift force in this case has a direction opposite to the shear induced lift force on a small bubble. For this reason, large bubbles tend to move to the pipe core region resulting in a core void maximum whereas a near-wall void peak is measured for small bubbles. The radial separation of small and large bubbles cannot be predicted by the homogeneous MUSIG model. This has been shown to be a key mechanism for the establishment of a certain flow regime as discussed earlier in chapter 2.

3.2. New strategies – the inhomogeneous MUSIG model

A combination of the consideration of different dispersed phases and the algebraic multiple size group model was proposed to combine both the adequate number of bubble size classes for the simulation of coalescence and breakup and a limited number of dispersed gaseous phases to limit the computational effort (Krepper et al. 2005). The inhomogeneous MUSIG model was developed in cooperation with ANSYS CFX and is implemented in CFX-10 (Shi et al. 2004, Zwart et al. 2003, Frank et al. 2005).

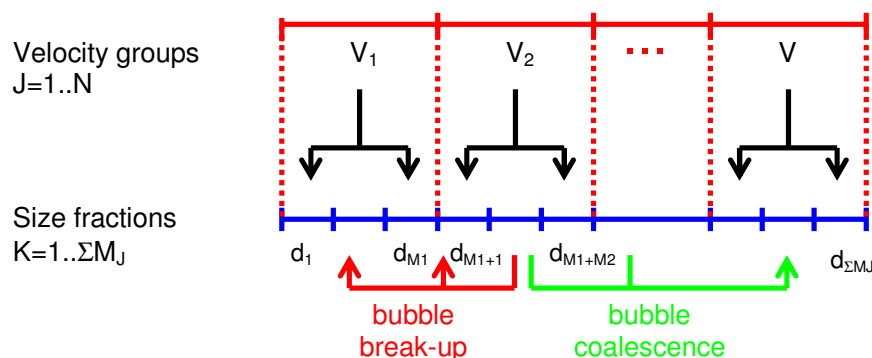


Figure 6: Improvement of the polydispersed approach: The size fractions M_j are assigned to the velocity field V_j

In the inhomogeneous MUSIG model the gaseous disperse phase is divided into a number N of so-called velocity groups (or phases), where each of the velocity groups is characterized by its own velocity field. Further, the overall bubble size distribution is represented by dividing the

bubble diameter range within each of the velocity groups j in a number M_j $j=1..N$ bubble sub-size fractions. The population balance model considering bubble coalescence or bubble breakup is applied to the sub-size groups (see Fig. 6). Hence the mass exchange between the sub-size groups can exceed the size ranges assigned to the velocity groups resulting in mass transfer terms between the different phases or velocity groups.

The lower and upper boundaries of bubble diameter intervals for the bubble size fractions can be controlled by either an equal bubble diameter distribution, an equal bubble mass distribution or can be based on user definition of the bubble diameter ranges for each distinct bubble diameter fraction. The subdivision should be based on the physics of bubble motion for bubbles of different size, e.g. different behavior of differently sized bubbles with respect to lift force or turbulent dispersion. Therefore, it can be suggested that in most cases $N=2$ or 3 velocity groups are sufficient in order to capture the main phenomena in bubbly or slug flows.

The continuity equation for the gaseous dispersed phase j can then be written as:

$$\frac{\partial}{\partial t}(\alpha_j \rho_g) + \nabla \cdot (\alpha_j \rho_g \vec{U}_j) = S_j \quad (5)$$

the momentum equation for the j -th gaseous phase has the form:

$$\begin{aligned} \frac{\partial}{\partial t}(\alpha_j \rho_g \vec{U}_j) + \nabla \cdot (\alpha_j \rho_g \vec{U}_j \times \vec{U}_j) = \nabla \cdot (\alpha_j \mu_g (\nabla \vec{U}_j + (\nabla \vec{U}_j)^T)) \\ - \alpha_j \nabla p + \alpha_j \rho_g \vec{g} + \vec{M}_j + \vec{S}_{Mj} \end{aligned} \quad (6)$$

with

$$\vec{F}_j = \vec{F}_{j,D} + \vec{F}_{j,L} + \vec{F}_{j,W} + \vec{F}_{j,TD} \quad (7)$$

where α_j , ρ_g , μ_g are the void fraction, density and viscosity of the gas and \vec{F}_j represents the sum of interfacial forces like the drag force $F_{j,D}$, lift force $F_{j,L}$, wall lubrication force $F_{j,W}$ and turbulent dispersion force $F_{j,TD}$. The term \vec{S}_{Mj} represents the transfer of gaseous phase momentum between different velocity groups due to bubble breakup and coalescence processes that causes bubbles of certain size to switch to a different velocity group (secondary momentum transfer due to mass transfer).

Additional for each sub-size fraction, i , ($i=1..M_j$) in the velocity group j $f_i \alpha_j$ the continuity equation has to be solved:

$$\frac{\partial}{\partial t}(f_i \alpha_j \rho_g) + \nabla \cdot (f_i \alpha_j \rho_g \vec{U}_j) = S_{ij} \quad (8)$$

The source terms S_{ij} represent the local transfer of gaseous phase mass due to bubble breakup and coalescence processes. They can be assigned to S_k , which are the elements of the population balance model. Note that in the above equations the index j extends over the range $1..N$ and the index k over the range $1.. \sum_{j=1}^N M_j$. The population balance equations have then the form:

$$S_k = B_{k,B} - D_{kB} + B_{k,C} - D_{kC} \quad (9)$$

where $B_{k,B}$ is the bubble birth rate due to breakup of larger bubbles, $D_{k,B}$ is the bubble death rate due to breakup of bubbles from size group k into smaller bubbles, $B_{k,C}$ is the bubble birth rate into size group k due to coalescence of smaller bubbles to bubbles belonging to size group k and finally $D_{k,C}$ is the bubble death rate due to coalescence of bubbles from size group k with other bubbles to even larger ones. The inhomogeneous MUSIG model approach does not presume a certain coalescence or breakup model. As an example the validation calculations presented in the chapter 4 and 5 were performed applying the breakup model of Luo and Svendsen (1996) and the bubble coalescence model of Prince and Blanch (1990).

4. SIMULATING TWO PHASE FLOW IN VERTICAL PIPES

Gas-liquid flow in vertical pipes is a very good object for studying the phenomena of gas-liquid two-phase flows. In case of bubbly flows the bubbles move under well determined boundary conditions, resulting in a shear field of constant and well-known structure where the bubbles rise for a comparatively long time. This allows studying the lateral motion of the bubbles in a shear flow by comparing gas distributions measured at different heights.

4.1. Air Water Flow

In the TOPFLOW test, bubbles were injected from the side walls through 4 mm nozzles into a tube of diameter 195.3 mm. The bubble size distribution near the inlet shows large fractions of large bubbles (blue size distribution left side). During the upward flow through the tube the size distribution is shifted towards lower values. Thus the development of the bubble size distribution is mainly determined by fragmentation processes. Bubble coalescence plays only a minor role at the flow conditions of the experimental test. Fig. 7 shows the bubble size distribution and radial gas profiles for the test case TOPFLOW 118 for a quite low distance from the gas injection of 0.335 m and at a distance of 7.802 m. Note that only two dispersed phases were defined for the numerical model. 20 sub-size groups were then specified, where the first 2 sub-size groups are assigned to the first dispersed phase and the other 18 are assigned to the second dispersed phase. The bubble size diameter was defined up to 60 mm, the size step between the sub-size groups is equal to 3 mm. Test calculations have shown, that setting the breakup coefficient to $F_B=0.25$ and the coalescence coefficient to $F_C=0.05$ yields the best agreement for this flow regime of air-water flow in vertical pipes. Both the shift of the bubble size distribution (Fig. 7 left side) and the core peak gas volume fraction profile are well reproduced by the calculations.

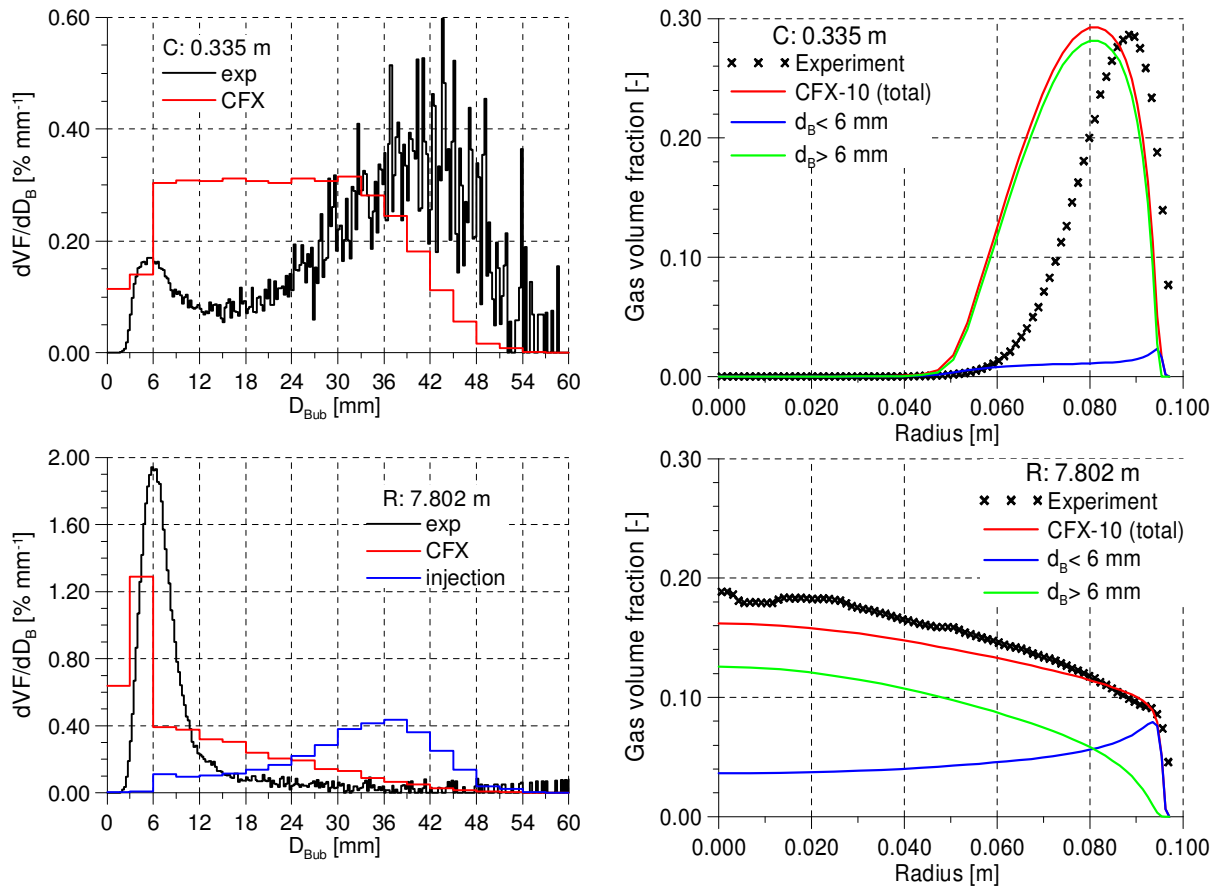


Figure 7: Bubble size distribution (left) and the radial gas fraction profiles (right) of the simulation of the test case TOPFLOW 118 at the distance levels from the gas injection C and R ($J_L=1.017$ m/s; $J_G=0.2194$ m/s) (Breakup coefficient $F_B=0.25$, Coalescence coefficient $F_C=0.05$)

4.2. Steam Water Flow at Saturation Conditions

Besides the air-water tests at the TOPFLOW facility also steam-water tests at pressures up to 6.5 MPa were performed. As a first step the influence of mass transfer by condensation was limited by keeping saturation conditions. In chapter 2.1 it was shown, that the lift coefficient C_L changes its sign with increasing bubble size. For air/water flow at ambient conditions the critical bubble size, for which $C_L=0$ amounts to be 5.8 mm. The analysis of the correlation for the lift coefficient (eq. (3) given by Tomiyama (1998) shows, that with higher pressure the critical bubble size is shifted towards lower values (see Fig. 2). For steam/water at 6.5 MPa a value of about 3.5 mm and at 15 MPa of about 2 mm was found. These tendencies were confirmed by the TOPFLOW experiments (see Fig. 3, Prasser et al. 2007).

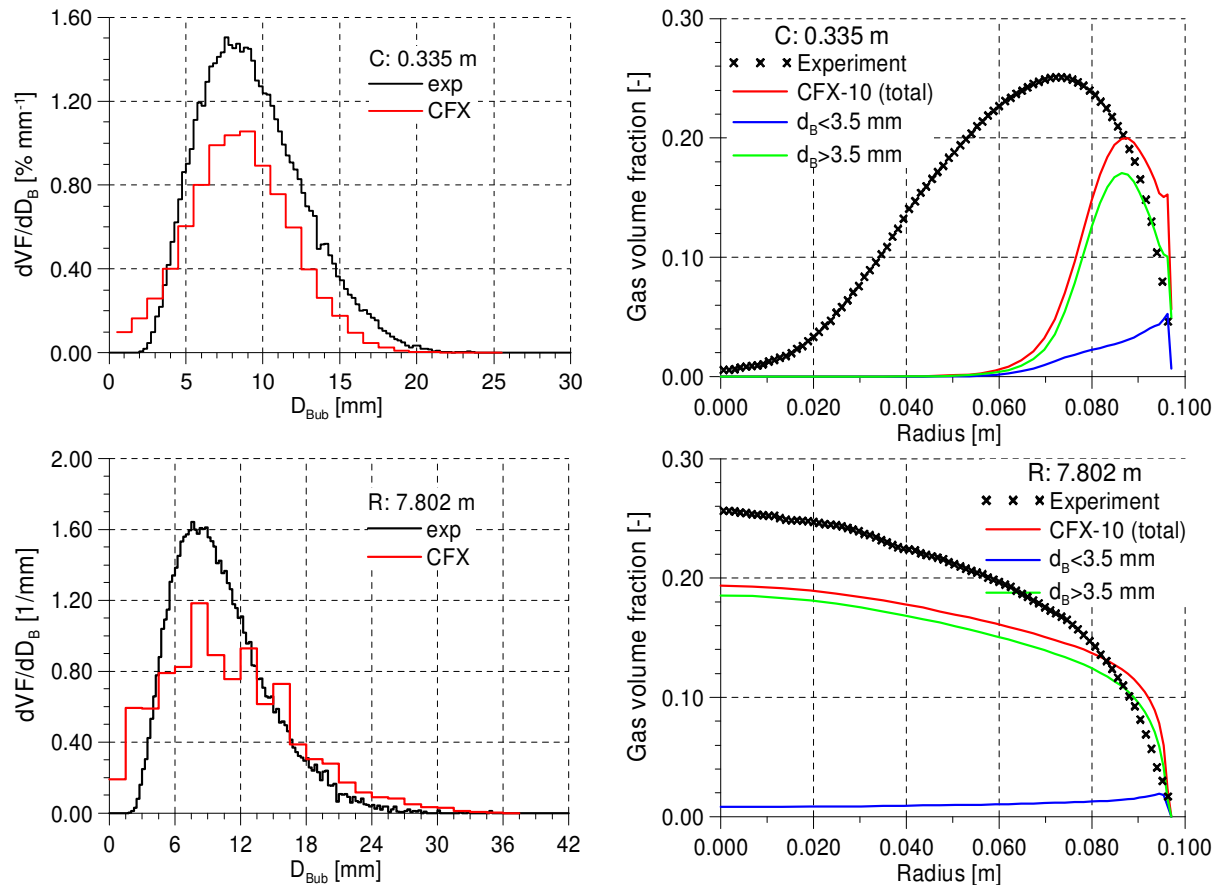


Figure 8: Bubble size distribution (left) and the radial gas fraction profiles (right) of the simulation of the test case TOPFLOW 118 at the distance levels from the gas injection C and R for saturated steam/water at 6.5 MPa ($J_L=1.017$ m/s; $J_G=0.2194$ m/s) (Breakup coefficient $F_B=0.025$, Coalescence coefficient $F_C=0.05$)

The changed fluid properties have influence on the calculated turbulence parameters of the liquid. For steam/water at 6.5 MPa the turbulence kinetic energy and the turbulence dissipation are almost doubled compared to air/water flow. Bubble fragmentation and bubble coalescence are strongly influenced by the turbulence dissipation of the liquid phase.

Fig. 8 presents the development of the bubble size distribution and of the radial volume fraction profiles for the steam/water test TOPFLOW-118. At 6.5 MPa steam water flow with superficial velocities $J_L=1.017$ m/s and $J_G=0.12194$ m/s was analyzed. 25 sub-size gas fractions assigned to two dispersed phases were simulated. The maximum considered bubble size was 37.5 mm. With equidistant bubble size distribution only the lowest two sub-size gas fractions were assigned to the first dispersed phase. For these flow conditions the critical bubble size for $C_L=0$ was 3.5 mm.

Whereas the factor for bubble coalescence was set like in the air/water simulations $F_C=0.05$ the fragmentation coefficient lead to a strong overestimation of bubble fragmentation. Consequently this coefficient in the further simulations was remarkably reduced to $F_B=0.025$. Fig. 8 shows, that applying the models with these tuned coalescence and fragmentation coefficients, a reasonable

simulation of the development of bubble size distribution and radial gas volume fraction profile is possible.

Compared to the air/water simulations (see Fig. 7) the migration of the bubbles from the injection at the wall to the centre of the tube is predicted to be slower in the steam/water case. Whereas in the air/water simulations the air moves too fast from the side wall injection into the pipe centre, in the steam/water tests the gas migration to the tube centre is underestimated. The reason could be the overestimated turbulent bubble dispersion force in the air/water cases. Caused by the other fluid properties the turbulent bubble dispersion force seems to be underestimated. Further investigations are necessary.

5. APPLICATION OF THE MODEL FOR THE FLOW AROUND AN OBSTACLE

In the TOPFLOW facility at FZD an experiment was performed, to study the flow field around an asymmetric obstacle. The obstacle had the form of a half moon shaped diaphragm and was arranged in a vertical tube having a diameter of DN200 (see Fig. 9). This is an ideal test case for CFD code validation, since the obstacle creates a pronounced three-dimensional two-phase flow field. Curved stream lines, which form significant angles with the gravity vector, a recirculation zone in the wake and a flow separation at the edge of the obstacle are common flow phenomena in industrial components and installations.

The wire-mesh technology was applied to measure the gas volume fraction and the gas velocity in different distances up- and downstream the obstacle. The sensors provide detailed data on the instantaneous flow structure with a high resolution in space and time. In particular, they allow visualizing the structure of the gas-liquid interface.

Pre-test calculations using CFX-10 and applying a monodispersed bubble size approach were performed for the conditions of test run 074 ($J_L = 1.017$ m/s, $J_G = 0.0368$ m/s) (see Prasser et al. 2005, Frank et al. 2007). In the calculation, a fluid domain was modeled 1.5 m upstream and downstream the obstacle. Half of the tube including a symmetry boundary condition set at the xz-plane of the geometry was simulated. In the present paper the inhomogeneous model approach was applied to air/water obstacle experiments run 096 ($J_L = 1.017$ m/s, $J_G = 0.0898$ m/s) and run 097 ($J_L = 1.611$ m/s, $J_G = 0.0898$ m/s). In the presented calculations for run 096 and run 097 25 respectively 20 sub-size gas fractions representing equidistant bubble sizes up to 25 mm respectively 20 mm were simulated, assigned to 2 dispersed gaseous phases. The first 6 size groups were assigned to the first gaseous phase (or velocity group) and the remaining size groups were assigned to the second gaseous phase. The bubble size distribution measured at the largest upstream position was set as an inlet boundary condition for the calculation.

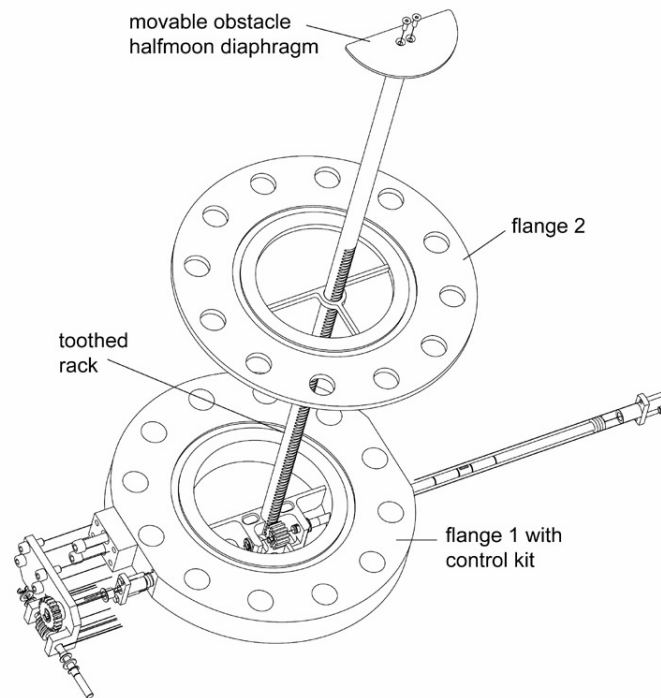


Figure 9: Sketch of the movable obstacle with driving mechanism - a half-moon shaped horizontal plate mounted on top of a toothed rod

5.1. The main observed phenomena

Like in the pretest calculations, the steady-state ANSYS CFX calculations applying the inhomogeneous MUSIG model could reproduce all qualitative details of the flow structure of the two-phase flow field around the diaphragm for the low gas fraction of run 074 .

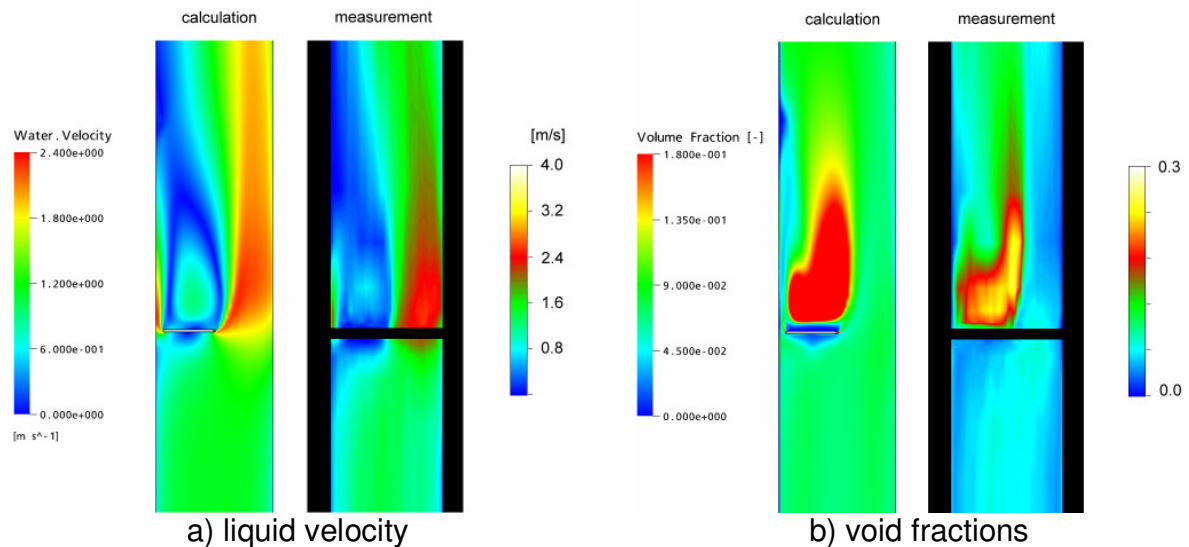


Figure 10: Comparison of time averaged calculated (left) and measured (right) values up- and downstream of the obstacle in the air-water test run 096, $J_L = 1.017$ m/s, $J_G = 0.0898$ m/s

The ANSYS CFX simulation results have been compared to three-dimensional wire-mesh sensor data in Fig 10. The water velocity and the total gaseous void fraction are presented. Like for the pretest calculations - also here for the test with higher gas fractions - all qualitative details of the structure of the two-phase flow field around the obstacle could be reproduced.

Shortly behind the obstacle a strong vortex of the liquid combined with the accumulation of gas is found. The measured and calculated shape and extension of the recirculation area agree very well. Upstream the obstacle a stagnation point with lower gas content is seen in experiment and calculation. Details, like the velocity and void fraction maxima above the gap between the circular edge of the obstacle and the inner wall of the pipe are also found in a good agreement between experiment and calculation. In the unobstructed cross sectional part of the tube a strong jet is established.

5.2. Phenomena in the wake of the obstacle

More detailed understanding of the flow situation can be gained, comparing the results of the inhomogeneous MUSIG model. According to the applied bubble fragmentation model of Luo and Svendsen (1996), bubble fragmentation can be expected in regions showing high turbulent eddy dissipation. Fig. 11 presents maximum values of the turbulent eddy dissipation at the edges of the obstacle. At the same time the applied bubble coalescence model of Prince and Blanch (1990) indicates strong importance of coalescence in regions of bubble accumulation i.e. in the wake behind the obstacle. Both bubble coalescence (see gas accumulation shown in Fig. 10) and bubble breakup (see distribution of turbulence dissipation Fig. 11), which might partially compensate each other, are expected shortly behind the obstacle.

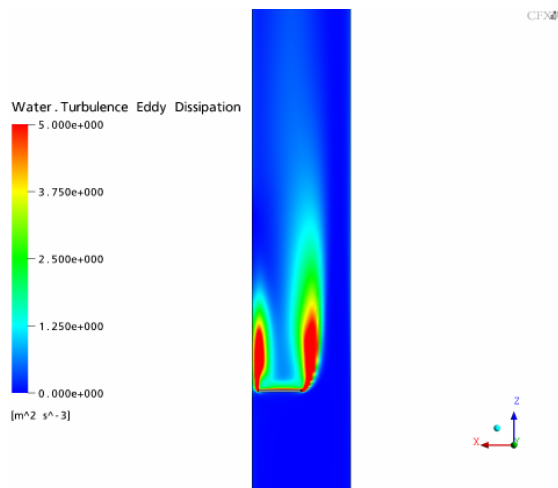


Figure 11: Calculated turbulence eddy dissipation (run 096)

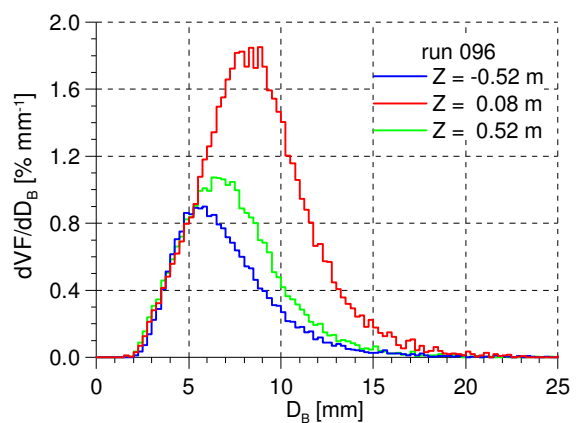


Figure 12: Measured bubble size distribution for run 096

Fig. 12 shows measured cross sectional averaged bubble size distributions upstream ($z = -0.52\text{m}$), shortly behind ($z = 0.08\text{m}$) and downstream the obstacle ($z = 0.52\text{m}$). In the bubble accumulation zone at $z = 0.08\text{m}$ the cross sectional average shows a shift towards larger bubbles. The

calculated bubble size distributions (see Fig. 13 for the run 096 and Fig. 14 for run 097) however show a shift of the mean bubble diameter towards smaller bubbles shortly behind the obstacle. In the calculations the bubble breakup is overestimated. This disagreement was found not solvable by simple changes of breakup or coalescence coefficients, which were set here to $F_B=F_C=0.05$. Similar deviations would arise at other locations of the flow domain.

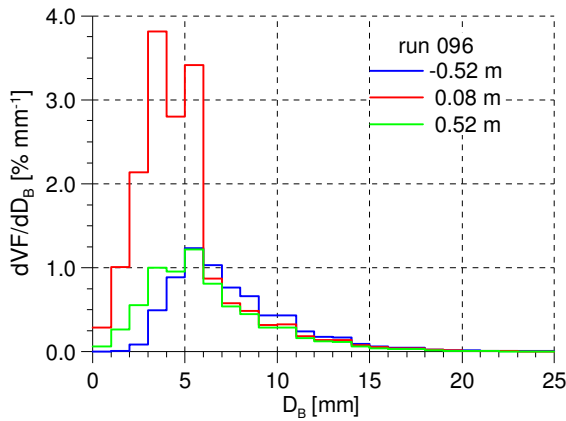


Figure 13: Calculated bubble size distributions for run 096 ($J_L=1.017$ m/s, $J_G=0.0898$ m/s)

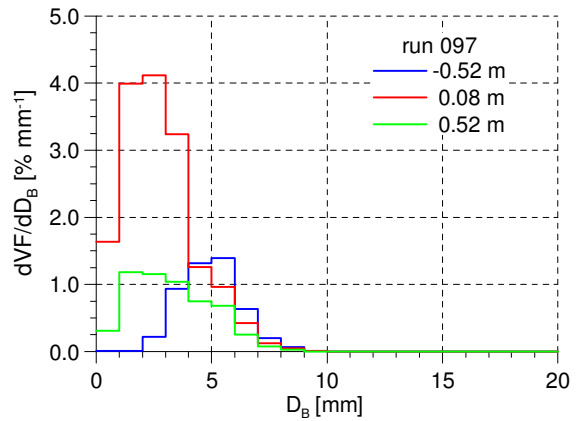


Figure 14: Calculated bubble size distributions for run 097 ($J_L=1.611$ m/s, $J_G=0.0898$ m/s)

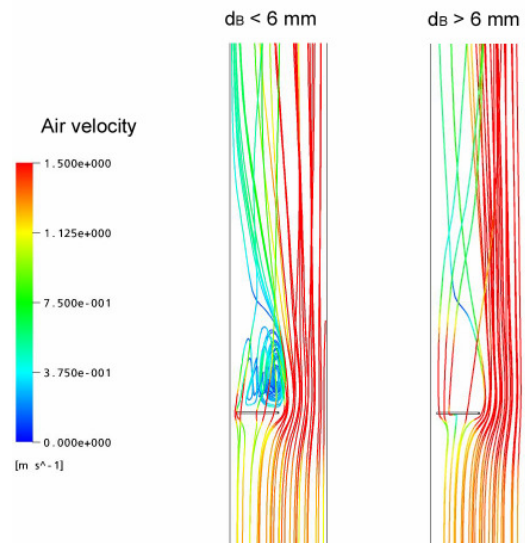


Figure 15: Streamlines for small (left) and large (right) bubbles (run 096)

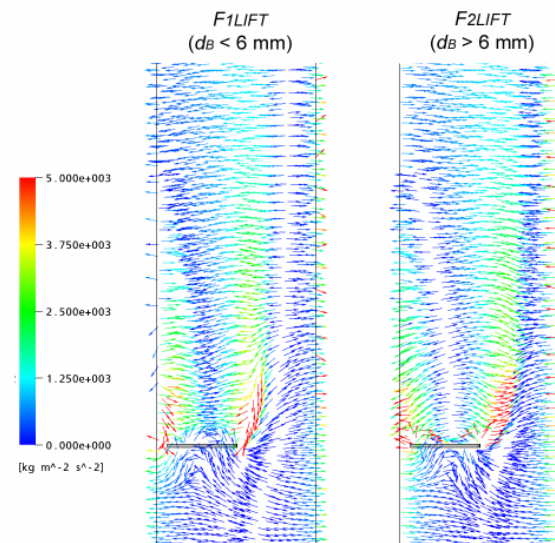


Figure 16: Bubble lift force vectors for the different gas velocity groups (run 096)

More detailed effects of lateral motion of small and large bubbles can be revealed by studying bubble streamlines and by analyzing lift forces acting on bubbles of different size. On the one hand side the liquid velocity flow field generates a lift force field which transports the small bubbles into the region behind the obstacle (see Fig. 15 for the bubble streamlines and Fig. 16 for the lift force arrows). On the other hand side, the air accumulation in the wake region leads to

bubble coalescence and the generation of large bubbles. This phenomenon is underestimated in the calculations. Figs. 15 and 17 show very well, how the small bubbles are being transported behind the obstacle. In the experiments larger bubbles are created by coalescence in this region. In the calculations however, bubble coalescence is exceeded in this region by bubble fragmentation. Caused by the lift force, large bubbles are redirected into the downstream jet (see Fig. 17) once they can be formed in the wake by coalescence. The streamline representation (see Fig. 15) clearly shows this phenomenon for large bubbles already present in the upstream flow.

5.3. Phenomena in the jet

In the cross sectional area beside the obstacle a strong jet is established creating strong shear flow. The resulting phenomena are more pronounced with increasing water velocity. Therefore, run 097 is considered, where the liquid velocity was increased to $J_L = 1.611$ m/s. Fig. 18 presents measured and calculated cross sectional gas fraction distributions for this run. In the most downstream cross section of the measurements an almost gas bubble free region is found. This effect is seen in almost all air/water measurements but not in the steam/water tests. The streamline representation of the calculations however (Fig. 15 for run 096, which is fairly similar to run 097), indicate large bubbles being directed into the jet caused by the lift force.

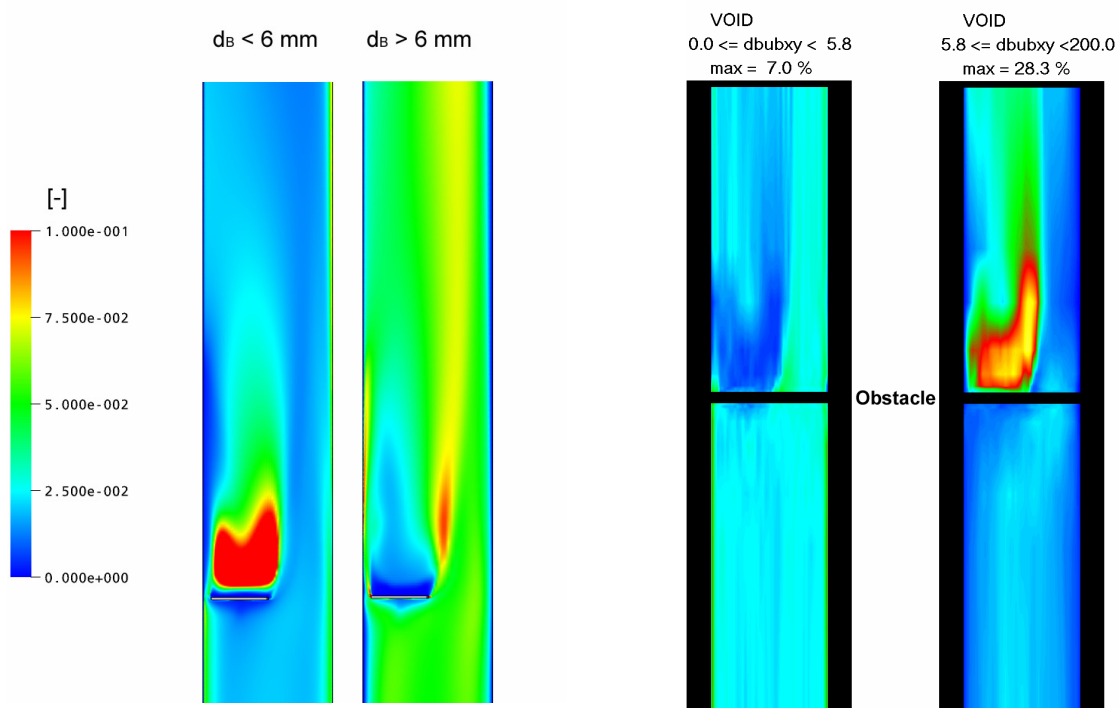


Figure 17: Calculated (left) and measured (right) gas distributions up- and downstream of the obstacle resolved to bubble size classes (run 096 $J_L = 1.017$ m/s, $J_G = 0.0898$ m/s)

This discrepancy between experiment and calculation can possibly be explained by the strong water velocity gradient near the jet. This strong shear flow induces bubble fragmentation which is not yet considered in the model of Luo and Svendsen (1996). In the tests, the big bubbles

migrate towards the jet, but are fragmented at the relatively sharp boarder of this jet. Only a small fraction of the small bubbles created by this breakup process can enter the jet by action of the turbulent dispersion force.

6. SUMMARY

Applying the inhomogeneous MUSIG approach, a more deep understanding of the flow structure is possible. For upward two phase flow in vertical pipes the core peak in the cross sectional gas fraction distribution could be reproduced very well. For complex flows the general structure of the flow could be well reproduced in the simulations. This test case of the obstacle demonstrates the complicated relationship and interference between size dependent bubble migration, bubble coalescence and breakup effects for real flows. While the closure models on bubble forces, which are responsible for the simulation of bubble migration, are in agreement with the experimental observations, clear deviations occur for bubble coalescence and fragmentation. The presently applied models describing bubble fragmentation and coalescence could be proven as weak points in numerous CFD analyses of vertical upward two phase pipe flow. Since these bubble breakup and coalescence models depend to a large extent on the turbulence properties of the two-phase flow, which could not be measured or validated in the pipe flow test cases, it has further to be investigated, whether the currently used multiphase flow turbulence models deliver appropriate and verifiable quantities which can be used for the description of bubble dynamics processes. Further work will be directed to these subjects in the near future.

ACKNOWLEDGMENTS

The work is carried out as a part of current research projects funded by the German Federal Ministry of Economics and Labour, project numbers 150 1265 and 150 1271. The authors express their gratitude to the technical TOPFLOW team.

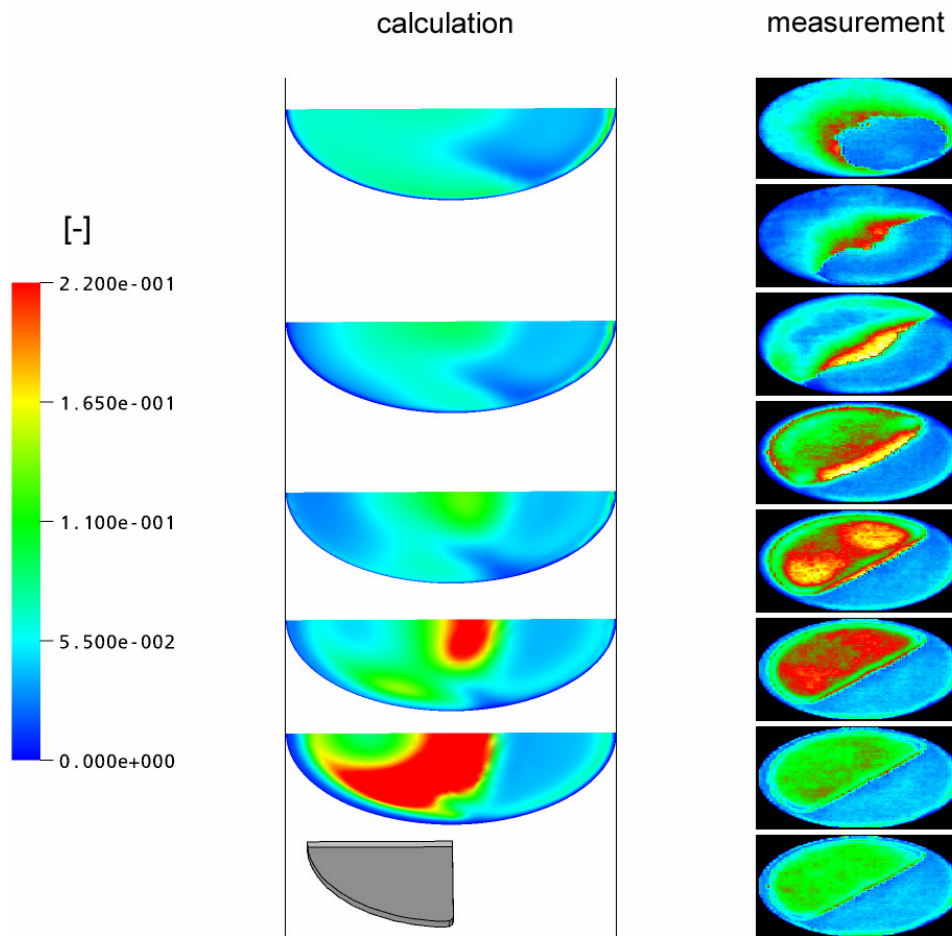


Figure 18: Calculated (left) and measured (right) cross-sectional distributions of gas volume fraction downstream the obstacle (run 097 JL = 1.611 m/s, JG = 0.0898 m/s) Calculations (obstacle shown), distances at $z=0.08$ m, 0.16 m, 0.25 m, 0.37 m and 0.52 m Measurements (obstacle in the upper left area) distances at $z=0.01$ m, 0.015 m, 0.02 m, 0.04 m, 0.08 m, 0.16 m, 0.25 m and 0.52 m

REFERENCES

1. Bothe, D., M. Schmidtke, H.-J. Warnecke (2006) VOF-Simulation of the Lift Force for Single Bubbles in a Simple Shear Flow, Chem. Eng. Technol. 29, No. 9, 1048–1053
2. Burns, A. D., T. Frank, I. Hamill J.-M. Shi, The Favre Averaged Drag Model for Turbulent Dispersion in Eulerian Multi-Phase Flows, 5th International Conference on Multiphase Flow, ICMF'04, Yokohama, Japan, May 30–June 4, 2004, Paper No. 392.
3. Ervin, E.A., Tryggvason, G. (1997). The rise of bubbles in a vertical shear flow, J.I of Fluids Engineering, vol. 119, pp. 443-449.

4. Frank, T., Zwart, P.J., Shi, J.-M., Krepper, E., Rohde, U. (2005). Inhomogeneous MUSIG Model – a Population Balance Approach for Polydispersed Bubbly Flows, International Conference “Nuclear Energy for New Europe 2005”, Bled, Slovenia, September 5-8, 2005.
5. Frank, Th., Zwart, P.J., Krepper, E., Prasser, H.-M., Lucas, D., (2006). Validation of CFD models for mono- and polydisperse air-water two-phase flows in pipes, OECD/NEA International Workshop on The Benchmarking of CFD Codes for Application to Nuclear Reactor Safety (CFD4NRS), 05.-09.09.2006, Garching, Deutschland, OECD/NEA, 05.-09.09.2006, Garching, Germany.
6. Frank, Th., H.-M. Prasser, M. Beyer, S. Al Issa. Gas-Liquid Flow around an Obstacle in a Vertical Pipe – CFD Simulation and Comparison to experimental Data, 6th Int. Conf. on Multiphase Flow Leipzig 2007, paper 135
7. Krepper, E.; Lucas, D.; Prasser, H.-M. (2005) On the modelling of bubbly flow in vertical pipes, Nuclear Engineering and Design 235 (2005) 597-611
8. Lo S. (1996). Application of the MUSIG model to bubbly flows, AEAT-1096, AEA Technology, June 1996.
9. Luo, H. and Svendsen, H.F. (1996), Theoretical model for drop and bubble break-up in turbulent flows, AIChEJ, 42, 5, pp. 1225-1233
10. Prasser, H.-M., Krepper, E., Lucas, D., (2002). Evolution of the two-phase flow in a vertical tube - decomposition of gas fraction profiles according to bubble size classes using wire-mesh sensors. International Journal of Thermal Sciences, 41 (2002) 17-28.
11. Prasser, H.-M., Frank, T., Beyer, M., Carl, H., Pietruske, H., Schütz, P. (2005), Gas-liquid flow around an obstacle in a vertical pipe experiments and CFD simulation, Annual Meeting on Nuclear Technology, Nuremberg
12. Prasser, H.-M.; Beyer, M.; Carl, H.; Gregor, S.; Lucas, D.; Pietruske, H.; Schütz, P.; Weiss, F.-P. (2007) Evolution of the structure of a gas-liquid two-phase flow in a large vertical pipe, Nuclear Engineering and Design (accepted for publication)
13. Prince, M.J. and Blanch, H.W. (1990), Bubble coalescence and break-up in air-sparged bubble columns, AIChEJ, 36, No 10, pp. 1485-1499
14. Shi, J.-M., Zwart, P.-J., Frank, T., Rohde U. and Prasser, H.-M. (2004). Development of a multiple velocity multiple size group model for poly-dispersed multiphase flows. In Annual Report of Institute of Safety Research. Forschungszentrum Rossendorf, Germany, 2004.
15. Tomiyama, A. Sou, I. Zun, I. Kanami, N. Sakaguchi, T. (1995). Effects of Eötvös number and dimensionless liquid volumetric flux on lateral motion of a bubble in a laminar duct flow, Advances in Multiphase Flow, pp. 3-15.
16. Tomiyama A. (1989): “Struggle with computational bubble dynamics”, ICMF’98, 3rd Int. Conf. Multiphase Flow, Lyon, France, pp. 1-18, June 8.-12. 1998.
17. Wellek, R.M., Agrawal, A.K., Skelland, A.H.P., (1966). Shapes of liquid drops moving in liquid media, AIChE Journal, vol. 12, pp. 854-860.
18. Zwart, P., A. Burns, A. and Montavon C.. (2003). Multiple size group models. Technical report, AEA Technology plc, November, 2003. CFX-5.7.